ACS Catalysis

Research Article

pubs.acs.org/acscatalysis

Rutile Crystallites Isolated from Degussa (Evonik) P25 TiO_2: Highly Efficient Photocatalyst for Chemoselective Hydrogenation of Nitroaromatics

Yasuhiro Shiraishi,*[,†] Hiroaki Hirakawa,[†] Yoshiki Togawa,[†] Yoshitsune Sugano,[†] Satoshi Ichikawa,[‡] and Takayuki Hirai[†]

[†]Research Center for Solar Energy Chemistry, and Division of Chemical Engineering, Graduate School of Engineering Science, Osaka University, Toyonaka 560-8531, Japan

[‡]Institute for NanoScience Design, Osaka University, Toyonaka 560-8531, Japan

Supporting Information

ABSTRACT: We report that the rutile crystallites, isolated from Degussa (Evonik) P25 TiO_2 by a hydrofluoric acid treatment, behave as a highly efficient photocatalyst for hydrogenation of nitroaromatics. Photoirradiation (λ >300 nm) of the isolated rutile particles with alcohol as a hydrogen source successfully promotes chemoselective hydrogenation of nitroaromatics to anilines, with an activity higher than that of commercially available rutile TiO_2. The high activity of the isolated rutile particles is due to the specific distribution of structural defects (oxygen vacancy sites) on the particles. These particles contain a relatively small number of inner defects behaving as recombination centers for photoformed electron (e^-) and positive hole (h^+) pairs, and a relatively large number of surface defects behaving as reduction sites for nitroaromatics. Photoexcitation of the isolated particles therefore promotes efficient charge separation between e^- and h^+, and facilitates rapid reduction of nitroaromatics adsorbed on the surface defects. This thus results in very high hydrogenation activity on the rutile particles isolated from P25 TiO_2.

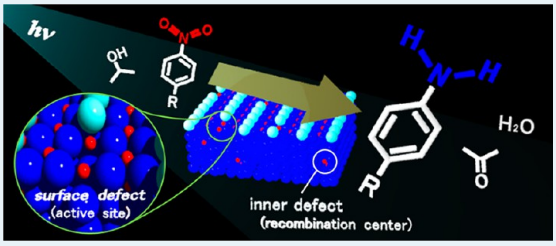

KEYWORDS: *photocatalysis, titanium dioxide, rutile, oxygen vacancy, structural defect*

INTRODUCTION

Functionalized anilines are versatile intermediate for the synthesis of pharmaceuticals, polymers, and fine chemicals.[1] They are generally produced by hydrogenation of nitroaromatics using stoichiometric or excess amounts of reducing agents with a concomitant formation of copious amount of waste.[2] Catalytic hydrogenation is therefore an ideal process; however, conventional systems with platinum-based catalysts and molecular hydrogen (H_2) also promote hydrogenation of other functionalities such as vinyl and carbonyl groups, resulting in poor chemoselectivity.[3] There are only a few catalytic systems of chemoselective nitro hydrogenation.[4−9] In addition, these systems require high H_2 pressure (>5 bar), high reaction temperature (>373 K), and noble metal catalyst such as gold and silver. Alternative systems that promote chemoselective nitro hydrogenation under milder reaction conditions (room temperature and atmospheric pressure) without noble metal are necessary for safe and clean synthesis of functionalized anilines.

Earlier, we reported that photoexcitation (λ >300 nm) of semiconductor TiO_2 with alcohol as a hydrogen source promotes chemoselective hydrogenation of nitroaromatics.[10] The reaction can be carried out at room temperature and atmospheric pressure without noble metal, and successfully produces various functionalized anilines with >93% selectivity. The most striking aspect of this system is that "rutile" TiO_2 particles are effective for efficient and selective nitro hydrogenation. It is well-known that TiO_2 has two common polymorphic forms: anatase and rutile. Anatase usually exhibits much higher photocatalytic activity than rutile,[11] and its activity is further improved by coupling with about 20% rutile, which is available as AEROXIDE P25 TiO_2 by Degussa (Evonik).[12] Both anatase and P25 TiO_2, however, show lower activity and selectivity than rutile TiO_2 for nitro hydrogenation.

X-ray photoelectron spectroscopy (XPS), diffuse-reflectance infrared Fourier transform (DRIFT) spectroscopy, and DR UV−vis spectroscopy of rutile TiO_2 revealed that the active sites for photocatalytic nitro hydrogenation on rutile TiO_2 are the Ti^{3+} atoms located at the surface defects. As shown in Scheme 1a, the rutile (110) surface is characterized by alternate rows of 5-fold coordinated Ti^{4+} atoms and bridging O^{2-} atoms (O_b) that run in the (001) direction.[13] Surface defects are the O_b vacancies, where two excess electrons associated with O_b are transferred to the empty 3d orbitals of neighboring Ti^{4+} atoms, producing two exposed Ti^{3+} atoms. As shown in Scheme 1b, these surface Ti atoms behave as an adsorption site for

Received: July 9, 2013
Revised: August 8, 2013
Published: September 6, 2013

   dx.doi.org/10.1021/cs400532p | ACS Catal. 2013, 3, 2318−2326

Scheme 1. (a) Surface and Inner Structure of Rutile TiO_2 (110), and (b) Photocatalytic Cycle for Hydrogenation of Nitrobenzene on the Surface Defect[a]

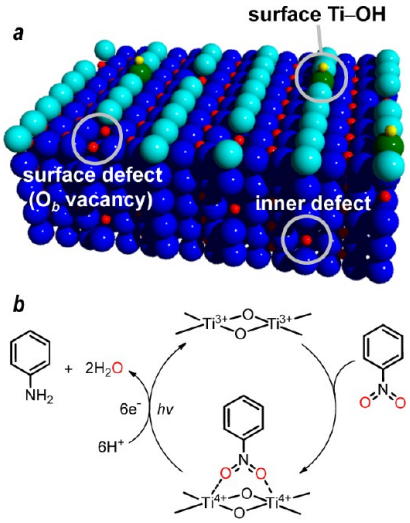

[a]The light blue and green spheres are O_b atoms that lie in the [001] azimuth. The parallel red spheres are Ti atoms and small yellow spheres are H atoms, respectively.

nitroaromatics via an electron donation to the oxygen atoms of nitro groups,[14] and as a trapping site for photoformed conduction band electrons.[15] These effects therefore facilitate rapid nitro-to-amine reduction on the photoactivated rutile TiO_2.

Next is the exploration of highly active rutile TiO_2 particles for rapid nitro hydrogenation. It is well-known that commercially available rutile TiO_2 are synthesized by the "wet process" (hydrolysis of Ti precursors followed by calcination).[16] In contrast, P25 TiO_2 is synthesized by the "dry process" (flame pyrolysis of gaseous $TiCl_4$),[17] and it is a mixture of anatase and rutile particles (ca. 80/20 w/w).[12] Herein, we report that the rutile particles, isolated from P25 TiO_2 by a hydrofluoric acid (HF) treatment, promote photocatalytic nitro hydrogenation with an activity higher than that of commercially available rutile TiO_2. DRIFT and DR UV–vis analysis was carried out to clarify the reason for high activity of the isolated rutile particles. Photocatalytic activity of rutile TiO_2 depends strongly on the number of surface defects as well as the number of inner defects on the particles (Scheme 1b). The rutile particles isolated from P25 TiO_2 have a defect distribution that differs significantly from the commercially available rutile particles synthesized by the wet process. The isolated rutile particles contain a relatively small number of inner defects behaving as recombination centers for photoformed electron (e^-) and positive hole (h^+) pairs, and a relatively large number of surface defects behaving as active sites for nitro hydrogenation. Photoexcitation of the isolated rutile particles therefore promotes efficient charge separation between e^- and h^+, and facilitates rapid reduction of nitroaromatics adsorbed on the surface defects, resulting in high activity for nitro hydrogenation.

RESULTS AND DISCUSSION

Preparation and Properties of Catalysts. HF solution dissolves anatase TiO_2 more easily than rutile;[18] therefore, rutile particles can easily be isolated from P25 by simple HF treatment. P25 TiO_2 particles (1 g) were stirred in water (50 mL) with different concentrations of HF (x wt %) for 24 h at 298 K. The resulting powders were washed thoroughly with water until the pH of solution becomes about 7 to remove HF and F^- and dried in vacuo for 12 h, affording HF(x)/P25 particles. As summarized in Table 1 (samples **2**–**4**), the percent recovery of particles decreases with an increase in HF concentration, suggesting that parts of P25 are dissolved in HF solution.

Table 1. Properties of TiO_2 and the Rate for Photocatalytic Hydrogenation of Nitrobenzene[a]

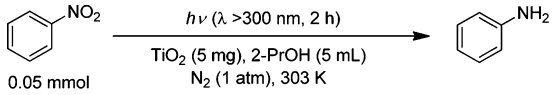

sample	catalyst	recovery/%[b]	crystalline phase[c]	S_{BET}/m^2 g^{-1}[d]	d_p/nm[e]	E_{bg}/eV[f]	v_i/μmol h^{-1}[g]	$N_{surface}$/μmol g^{-1}[h]	N_{total}/μmol g^{-1}[i]
1	P25[j]		A 83/R 17	57	27, 340	3.15	9.9		
2	HF(5)/P25	16	A 30/R 70	36	107	3.00	11.2		
3	HF(10)/P25	8	R	32	71	2.97	17.3	40.2	53.8
	first reuse[k]						17.5		
	second reuse[k]						16.7		
4	HF(15)/P25	6	R	38	61	2.95	7.1	10.4	49.4
5	JRC-TIO-6[j]		R	100	21	3.00	15.6	168.0	253.1
6	NS-51[l]		R	7	217	2.97	11.9	15.9	32.9
7	PT-101[m]		R	25	71	2.98	11.9	81.6	146.2
8	CR-EL[m]		R	7	245	2.95	11.4	11.1	22.0
9	Wako rutile		R	15	276	2.96	<0.1	1.9	19.9
10	HF(10)/JRC-TIO-6		R	114	14	2.98	10.4		

[a]Photoirradiation was carried out with a 2 kW Xe lamp (light intensity at 300–450 nm is 27.3 W m^{-2}). [b]Percent recovery of particles after HF treatment. [c]Determined by XRD analysis, where the ratio of anatase (A) and rutile (R) was determined with the equation; A (%) = $I_{A(101)}/(I_{A(101)} + 1.4I_{R(110)}) \times 100$ (ref 19). [d]Brunauer–Emmett–Teller surface area determined by N_2 adsorption/desorption analysis. [e]Particle diameter determined by DLS analysis. [f]Bandgap energies determined by a plot of the Kubelka–Munk function versus the energy of light absorbed. [g]Initial rate for aniline formation determined by dividing the amount of aniline formed during 2 h photoreaction by 2 (h). [h]Number of surface defects. [i]Number of total defects. [j]Japan Reference Catalyst supplied from Catalyst Society of Japan. [k]The catalyst was reused after simple washing with solvent. [l]Supplied from Toho Titanium Co., Ltd. (Japan). [m]Supplied from Ishihara Sangyo, Ltd. (Japan).

dx.doi.org/10.1021/cs400532p | ACS Catal. 2013, 3, 2318–2326

Figure 1 shows the X-ray diffraction (XRD) patterns of P25 and HF(x)/P25. Pure P25 exhibits distinctive diffractions

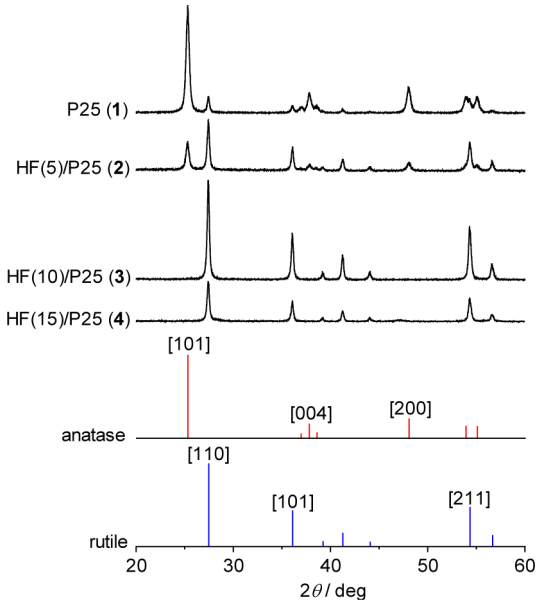

Figure 1. XRD patterns of respective TiO_2 particles and standard patterns for anatase (JCPDS 21-1272) and rutile (JCPDS 21-1276). The text in the parentheses denotes the sample number listed in Table 1. The XRD patterns for other rutile particles are summarized in Supporting Information, Figure S1.

assigned to anatase and rutile crystallites. As shown in Table 1 (sample **1**), the ratio of anatase and rutile phases for P25, determined by the intensity ratio,[19] is 83:17. HF treatment of P25 decreases the anatase diffractions because of the dissolution of anatase phase. HF(5)/P25 (sample **2**) still contains anatase (30%), but HF(10)/P25 (sample **3**) and HF(15)/P25 (sample **4**) exhibit solely rutile diffractions.

Figure 2 shows the DR UV−vis spectra of HF(x)/P25. The absorption edge of pure P25 is about 400 nm, and its bandgap energy is 3.15 eV (Table 1). HF treatment of P25 leads to a shift of the absorption edge to longer wavelength (ca. 420 nm), along with a decrease in the bandgap energy. This suggests that anatase crystallites with bandgap energy larger than rutile crystallites[20] are selectively dissolved in HF solution.

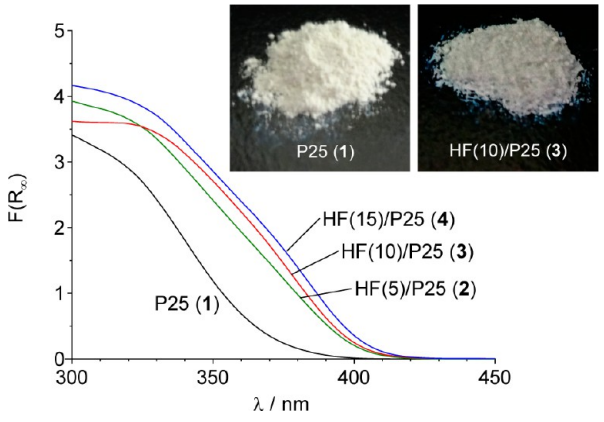

Figure 2. DR UV−vis spectra of HF(x)/P25. The spectra for other rutile TiO_2 particles are summarized in Supporting Information, Figure S2.

Figure 3 shows the typical transmission electron microscopy (TEM) images of TiO_2 particles. Pure P25 (Figure 3a) is a

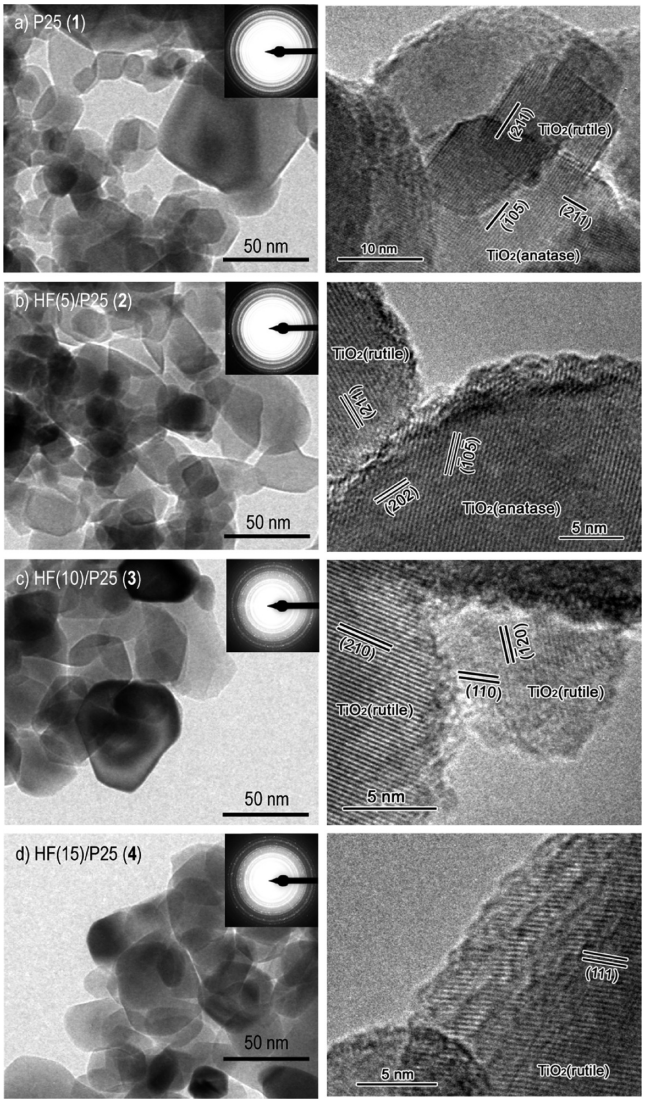

Figure 3. Typical (left) TEM and (right) high-resolution TEM images of HF(x)/P25. More images of HF(10)/P25 and HF(15)/P25 are summarized in Supporting Information, Figures S3 and S4, respectively.

mixture of small particles with 20−40 nm diameters and large particles with 60−100 nm diameters, which are assigned to anatase and rutile particles, respectively.[18] HF treatment of P25 (Figure 3b−d) leads to a disappearance of small particles, suggesting that anatase particles are indeed dissolved in HF solution. Most of the HF(10)/P25 particles are surrounded by a low indexed plane. In contrast, the shape of HF(15)/P25 is almost round, and the size of particles is smaller than that of HF(10)/P25. This means that parts of the rutile particles are decomposed by the treatment with higher concentration of HF.[21,22] These data suggest that the treatment of P25 with about 10% HF successfully isolates rutile particles while maintaining high crystallinity.

Figure 4 shows the distribution of particle size determined by dynamic laser scattering (DLS) analysis. As shown by the black line, pure P25 exhibits bimodal distribution with average diameters 27 and 340 nm, respectively. The smaller particles

dx.doi.org/10.1021/cs400532p | ACS Catal. 2013, 3, 2318−2326

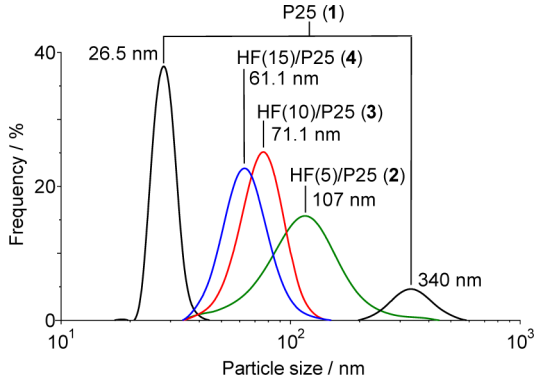

Figure 4. Size distribution of HF(x)/P25 particles determined by DLS analysis. The distributions of other rutile TiO_2 are summarized in Supporting Information, Figure S5.

are assigned to the dispersed anatase particles,[23] and the larger particles are the interwoven aggregates of anatase and rutile particles.[24] HF treatment of P25 leads to a disappearance of the dispersed anatase particles, along with a decrease in the size of aggregates. HF(10)/P25 shows monodispersed particle distribution with average diameter 71 nm, indicating that monodispersed rutile particles are isolated from P25 by the HF treatment.

Photocatalytic Activity. The activity of respective catalysts was tested by hydrogenation of nitrobenzene to aniline with 2-PrOH. Each respective catalyst (5 mg) was added to 2-PrOH (5 mL) containing nitrobenzene (10 mM), and the suspension was photoirradiated by a Xe lamp (λ >300 nm) with stirring under N_2 atmosphere (1 atm). The time-course profiles for aniline formation on the respective catalysts are shown in Supporting Information, Figure S6. It is noted that the absence of catalyst promotes almost no reaction. Table 1 summarizes the initial rate for aniline formation determined by 2 h photoreaction on the respective catalyst (v_f/μmol h^{-1}). The v_f of P25 (sample **1**) is 9.9 μmol h^{-1}. HF treatment of P25 increases the reaction rate; v_f of HF(5)/P25 (sample **2**) is 11.2 μmol h^{-1}, indicating that rutile TiO_2 is indeed effective for nitro hydrogenation.[10] HF(10)/P25 (sample **3**) exhibits much higher activity (17.3 μmol h^{-1}), whereas HF(15)/P25 (sample **4**) shows decreased activity (7.1 μmol h^{-1}). In the dark condition, HF(10)/P25 promotes almost no reaction, suggesting that photoexcitation of the catalyst initiates nitro hydrogenation.

It must be noted that the activity of HF(10)/P25 (sample **3**) is higher than that of commercially available rutile TiO_2 (samples **5**–**9**). It is well-known that photocatalytic activity of TiO_2 depends on their surface area; the catalyst with larger surface area shows enhanced activity.[25] The HF(10)/P25 catalyst (sample **3**) has a surface area (32 m^2 g^{-1}) much smaller than JRC-TIO-6 rutile TiO_2 (100 m^2 g^{-1}; sample **5**), but shows higher activity. In addition, as shown in Figure 5a, the plot of v_f versus the surface area for the respective TiO_2 (samples **3**–**9**) shows almost no relationship. These data suggest that the high photocatalytic activity of the rutile particles isolated from P25 cannot be explained by the surface area. It must also be noted that, as shown by the sample **10** (Table 1), JRC-TIO-6, treated with 10% HF solution, shows activity (10.4 μmol h^{-1}) much lower than that of pure JRC-TIO-6 (sample **5**; 15.6 μmol h^{-1}). This clearly indicates that HF treatment does not enhance photocatalytic activity, but the rutile particles contained in P25 inherently possess high activity. It is also note that, as shown in Table 1 (sample **3**), the HF(10)/P25 catalyst recovered after photoreaction, when reused for further reaction, shows almost the same activity as the virgin catalyst. This suggests that the catalyst is reusable without the loss of activity.

Chemoselective nitro hydrogenation is successfully promoted on HF(10)/P25. Table 2 summarizes the results for

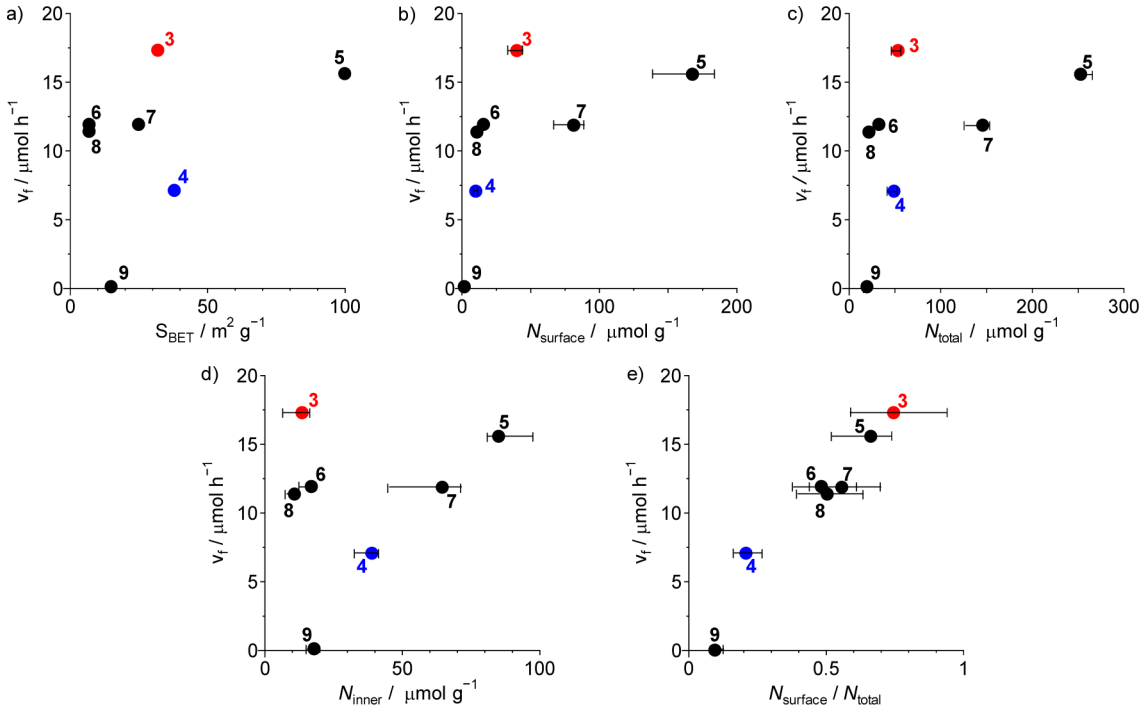

Figure 5. Relationship between v_f versus (a) S_{BET}, (b) $N_{surface}$, (c) N_{total}, (d) N_{inner}, and (e) $N_{surface}/N_{total}$ for respective rutile TiO_2 (sample **3**–**9**). The sample numbers correspond to those listed in Table 1

dx.doi.org/10.1021/cs400532p | *ACS Catal.* 2013, 3, 2318–2326

Table 2. Photocatalytic Hydrogenation of Nitroaromatics on HF(10)/P25 (sample 3) or JRC-TIO-6 (Sample 5) Catalyst[a]

entry	substrate	catalyst	solvent[b]	t / h[c]	substrate conv. / %[d]	product	product yield / %[d]
1[e]		HF(10)/P25	2-PrOH	3	97		94
2[e]		JRC-TIO-6			84		81
3[e]		HF(10)/P25	2-PrOH/toluene (1/9 w/w)	3	>99	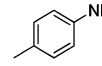	98
4[e]		JRC-TIO-6			78		76
5	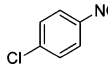	HF(10)/P25	2-PrOH/toluene (1/9 w/w)	4	>99	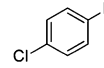	96
6		JRC-TIO-6			78		71
7	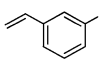	HF(10)/P25	2-PrOH/toluene (9/1 w/w)	6	>99	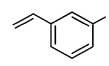	94
8		JRC-TIO-6			87		83
9	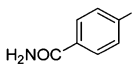	HF(10)/P25	2-PrOH/THF (5/5 w/w)	5	>99	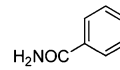	98
10		JRC-TIO-6			80		78
11	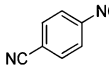	HF(10)/P25	2-PrOH/toluene (1/9 w/w)	5	>99	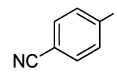	98
12		JRC-TIO-6			82		78
13[f]	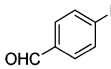	HF(10)/P25	2-PrOH/toluene (1/9 w/w)	5	>99	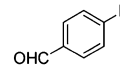	94
14[f]		JRC-TIO-6			91		85

[a]Reaction conditions: substrate (50 μmol), catalyst (10 mg), solvent (5 mL), temperature (303 K), N_2 (1 atm), Xe lamp (λ >300 nm). [b]Solvents were selected in respect to the solubility of substrates. [c]Photoirradiation time. [d]Determined by GC. [e]Catalyst (5 mg). [f]Substrate (25 μmol).

photoreaction of nitroaromatics with various substituents. All of the nitroaromatics are converted to the corresponding anilines with >94% yields even in the presence of reducible substituents. These activities are higher than those of JRC-TIO-6 rutile TiO_2 with larger surface area.[10] These results suggest that HF(10)/P25 promotes rapid and chemoselective nitro hydrogenation.

Figure 6 shows the time-dependent change in the amounts of substrate and products during photocatalytic reaction of

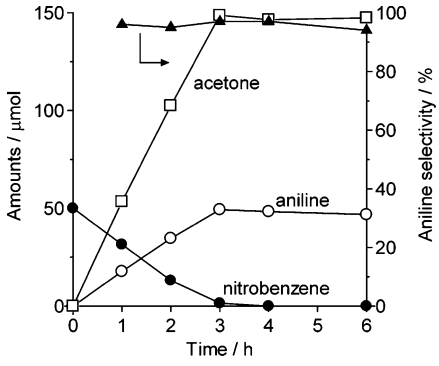

Figure 6. Time-dependent change in the amounts of substrate and products during photoreaction of nitrobenzene in 2-PrOH with HF(10)/P25 (sample **3**). The reaction conditions are identical to those in Table 1

nitrobenzene with the HF(10)/P25 catalyst. The substrate nitrobenzene (50 μmol) is quantitatively transformed to aniline by 3 h photoreaction, along with a formation of almost 3 equiv of acetone (150 μmol). This indicates that the H atoms of alcohol, removed by oxidation with photoformed h^+, are consumed quantitatively by the nitro-to-amine hydrogenation. Stoichiometric oxidation and reduction reactions therefore occur on the rutile particles isolated from P25, as is the case for commercially available rutile TiO_2,[10] as shown in Scheme 1b and as follows.

$$3(CH_3)_2CHOH + 6h^+ \rightarrow 3(CH_3)_2CO + 6H^+ \quad (1)$$

$$Ar{-}NO_2 + 6e^- + 6H^+ \rightarrow Ar{-}NH_2 + 2H_2O \quad (2)$$

Surface Defects as Active Reduction Site. The active site for photocatalytic reduction of nitroaromatics on rutile TiO_2 is the exposed Ti^{3+} atoms located at the surface defect (Scheme 1).[10] The Ti^{3+} atoms behave as adsorption sites for nitroaromatics and trapping sites for photoformed e^-, thus promoting rapid nitro-to-amine reduction. This suggests that the number of surface defects is probably an important factor affecting the photocatalytic activity of rutile TiO_2. The number of surface defects can be determined by DRIFT analysis of nitrobenzene adsorbed onto the catalysts in the gas phase.[10] Respective rutile particles (50 mg) were placed in a DR cell and evacuated (0.9 Pa) at 423 K for 3 h. Excess amount of nitrobenzene (16.5 μmol) was introduced to the cell at 303 K and left for 1 h. The cell was then evacuated (0.9 Pa) for 1 h to remove the physically adsorbed nitrobenzene. Figure 7 shows the DRIFT spectra of the nitrobenzene adsorbed onto the respective rutile TiO_2. Two absorption bands appear at 1522 and 1346 cm^{-1}. The 1522 cm^{-1} band is assigned to the asymmetric stretching vibration (ν_{asym}) of the nitro group adsorbed onto the surface Ti−OH group, which is inactive for nitro reduction.[10] In contrast, the 1346 cm^{-1} band is assigned to the symmetric stretching vibration (ν_{sym}) of the nitro group adsorbed onto the surface Ti^{3+} atoms,[26] which is the active site for nitro reduction. The number of nitrobenzene adsorbed onto the surface Ti^{3+} atoms can be determined by the intensity ratio of the respective bands. The number of surface Ti^{3+} atoms (surface defects) per gram catalyst ($N_{surface}$/μmol g^{-1}) is equal to twice the amount of adsorbed nitrobenzene.

The $N_{surface}$ values for respective rutile TiO_2 are summarized in Table 1. Figure 5b plots $N_{surface}$ versus the initial rate for

dx.doi.org/10.1021/cs400532p | ACS Catal. 2013, 3, 2318−2326

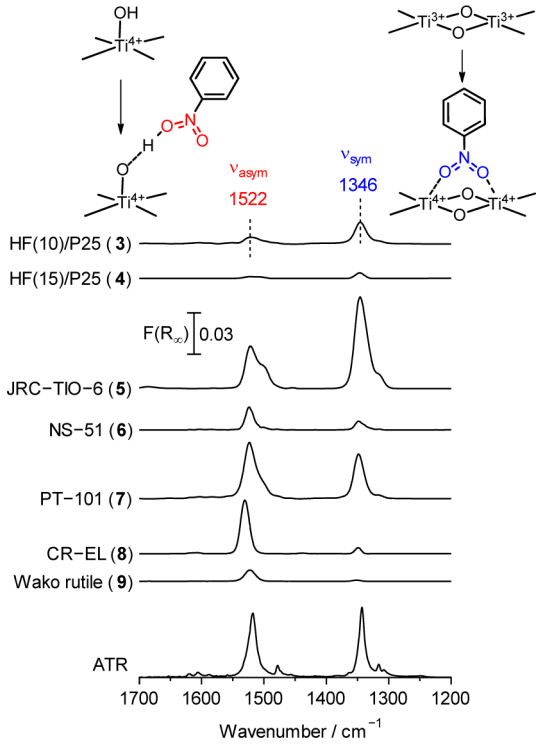

Figure 7. DRIFT spectra of nitrobenzene adsorbed onto the respective TiO_2 particles in the gas phase at 303 K. Attenuated total reflection (ATR) spectrum for nitrobenzene obtained at 303 K is also shown in the figure.

aniline formation (v_f) during photocatalytic reduction of nitrobenzene for the respective rutile TiO_2. The plotting data indicate that there is almost no relationship between these factors. In that, the HF(10)/P25 catalyst (sample **3**) with relatively smaller $N_{surface}$ value shows the highest activity. This suggests that the $N_{surface}$ value is not the sole factor affecting the phocatalytic activity of rutile TiO_2.

Surface and Inner Defects as Deactivation Sites. As shown in Scheme 1a, oxygen vacancies exist inside the TiO_2 particles as well as on the particle surface. These inner and surface defects create some energy levels around the midgap and behave as recombination centers for photoformed e^- and h^+, resulting in deactivation of photoexcited TiO_2.[27] This means that the inner defects behave as recombination centers, whereas the surface defects behave as active sites for reduction as well as recombination centers. This implies that the rutile particles with smaller number of defects would allow efficient charge separation between e^- and h^+. The number of inner defects (N_{inner}) or total defects (N_{total}) may therefore affect the photocatalytic activity.

As reported,[28] the total number of defects on TiO_2 can be determined by photocatalytic reduction of methyl viologen (MV^{2+}). TiO_2 particles (5 mg) were added to water (10 mL) containing triethanolamine (TEOA, 10%) as a h^+ scavenger, and the suspension was photoirradiated with stirring under Ar atmosphere at 298 K. After the photoreaction, a chloride salt of MV^{2+} (125 μmol) was added to the resulting blue suspension and stirred for 1 h in the dark at 298 K under Ar. The resulting solution was recovered by centrifugation and subjected to UV−vis absorption analysis. Figure 8 shows the absorption spectra of the solution recovered after photoreaction with PT-101 catalyst (sample **7**) followed by reaction with MV^{2+} as an

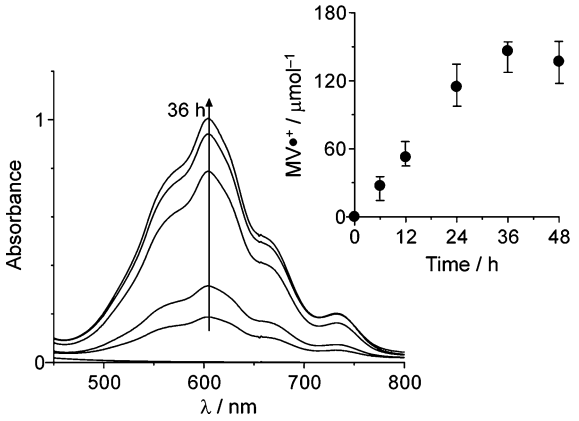

Figure 8. Time-dependent change in the absorption spectra of an aqueous solution obtained after photoreaction with TEOA and PT-101 catalyst (sample **7**) followed by reaction of MV^{2+} (1 h). (Inset) change in the amount of formed $MV^{\bullet+}$ with the photoirradiation time.

example. A distinctive absorption band appears at 606 nm, which is assigned to the radical cation of methyl viologen ($MV^{\bullet+}$), and its intensity increases with the photoirradiation time. During the photoreaction, the photoformed h^+ oxidizes TEOA, while the e^- reduces the Ti^{4+} atoms located at the surface or inner defects, producing Ti^{3+} atoms.

$$Ti^{4+}(\text{defect site}) + e^- \rightarrow Ti^{3+} \quad (3)$$

These accumulated e^- (Ti^{3+} sites) reduce MV^{2+} and produce $MV^{\bullet+}$.[29]

$$Ti^{3+} + MV^{2+} \rightarrow Ti^{4+} + MV^{\bullet+} \quad (4)$$

The amount of $MV^{\bullet+}$ produced, therefore, reflects the total number of Ti^{4+} atoms located at the defects on the particles. As shown in Figure 8, the increase in 606 nm band is saturated by >36 h photoirradiation. The saturated amount of $MV^{\bullet+}$ is identical to the total number of defects on the catalyst (N_{total}). Table 1 summarizes N_{total} of respective rutile TiO_2. The N_{total} values for the samples **5** and **8** are 253 and 22 μmol g^{-1}, which are very similar to the reported values (242 and 21 μmol g^{-1}),[30] indicating that the obtained N_{total} values are reliable. Figure 5c and d plot v_f versus N_{total} or the number of inner defects ($N_{inner} = N_{total} - N_{surface}$). There is almost no relationship between these factors, suggesting that the number of neither total defects nor inner defects is the sole factor affecting the photocatalytic activity of rutile TiO_2.

Effect of Inner and Surface Defects on the Activity. The above results suggest that the high photocatalytic activity of HF(10)/P25 cannot be explained by the number of surface, inner, or total defects. The surface defects behave as the active sites for reduction, whereas both surface and inner defects behave as the deactivation sites that promote recombination of photoformed e^- and h^+. The photocatalytic activity of rutile TiO_2 can therefore be explained by the number of surface defects relative to the number of total defects ($N_{surface}/N_{total}$). As shown in Figure 5e, the plot of v_f versus $N_{surface}/N_{total}$ clearly shows linear relationship, meaning that the catalyst with a smaller number of inner defects and a larger number of surface defects exhibits higher photocatalytic activity. This suggests that photocatalytic activity of rutile TiO_2 depends on the number of active sites relative to the number of deactivation sites on the catalyst, as follows:

dx.doi.org/10.1021/cs400532p | ACS Catal. 2013, 3, 2318−2326

$$v_f \propto \frac{N_{surface}}{N_{total}} \approx \frac{\text{the number of active sites}}{\text{the number of deactivation sites}} \quad (5)$$

As depicted in Scheme 2, the e^- and h^+ photoformed within TiO_2 migrate through the materials and appear on the surface.[27] During the migration, the e^- is trapped by the inner defect and deactivated by the recombination with h^+.[27] In contrast, the e^- successfully trapped by the surface defect promotes nitro reduction, whereas the parts of these Ti^{3+} sites are also deactivated by the recombination with h^+. This suggests that the smaller number of inner defects promotes efficient charge separation between e^- and h^+; in contrast, the larger number of surface defects provides a larger number of active sites for reduction. As a result of this, the catalyst with a smaller number of inner defects and a larger number of surface defects shows higher activity (eq 5), exhibiting linear relationship between v_f and $N_{surface}/N_{total}$ (Figure 5e). The higher photocatalytic activity of HF(10)/P25 particles is therefore due to their higher $N_{surface}/N_{total}$ value.

Scheme 2. Proposed Reaction and Deactivation Processes Occurring on the Photoactivated Rutile TiO_2

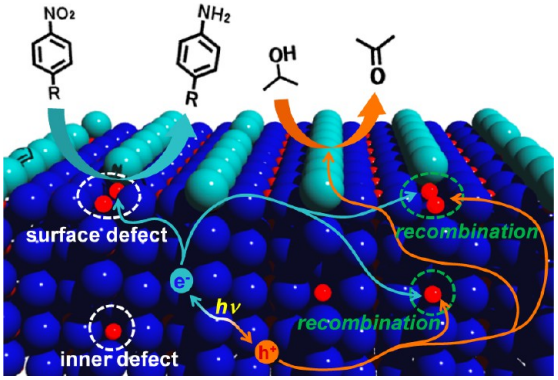

Distribution of Defects on TiO_2 Particles. The larger $N_{surface}/N_{total}$ value for the HF(10)/P25 particles is due to their structural specificity originated from the synthesis method, "dry process" (flame pyrolysis of gaseous $TiCl_4$). These particles contain a much smaller number of inner defects than commercially available rutile particles, while containing a relatively large number of surface defects. As reported,[31] the number of defects on the commercially available rutile particles synthesized by the "wet process" (hydrolysis of Ti precursors followed by calcination) depends on the particle size. Figure 9a shows the relationship between the particle size and N_{total} for respective rutile TiO_2. For commercially available TiO_2 (samples **5**–**9**), N_{total} decreases with an increase in the particle size. This means that the defect density in the particles decreases with the particle size increase. Larger TiO_2 particles are produced by calcination at higher temperature. During calcination, coalescence of small particles creates larger particles, along with a disappearance of defects by sintering. This thus creates larger particles with lower defect density (Figure 9a).[31] In contrast, as shown by the red symbol, N_{total} for HF(10)/P25 (sample **3**) does not follow this relationship, and the value is much lower than that expected from the particle size. In addition, as shown by the blue symbol, N_{total} for HF(15)/P25 (sample **4**) is also very low. These findings suggest that the rutile particles contained in P25 contain a much smaller number of defects than commercially available rutile TiO_2 synthesized by the wet process; in other words, these particles contain a much smaller number of deactivation sites for recombination of photoformed e^- and h^+.

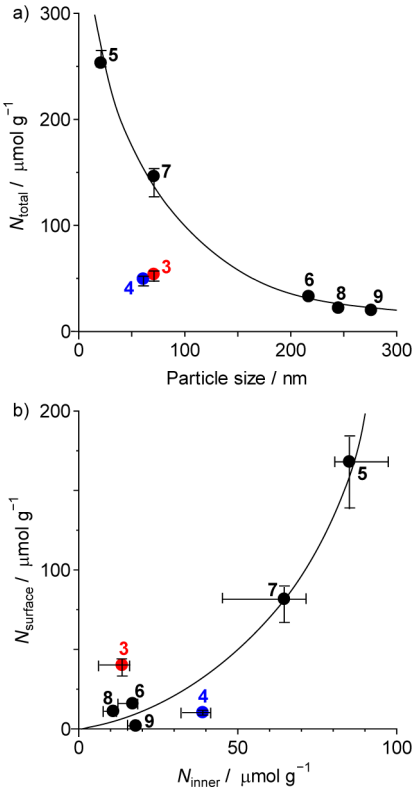

Figure 9. Relationship between (a) particle size and N_{total} and (b) N_{inner} and $N_{surface}$ for respective rutile TiO_2 (sample **3**–**9**). The sample numbers correspond to those listed in Table 1

Figure 9b shows the relationship between $N_{surface}$ and N_{inner} for respective rutile TiO_2. As reported,[31] for commercially available rutile particles (samples **5**–**9**), there is a positive correlation between these factors; $N_{surface}$ increases with an increase in N_{inner}. The larger increase in $N_{surface}$ than N_{inner} is due to the significant increase in the number of surface defects with an increase in the surface area associated with a particle size decrease. The positively correlated data suggest that both $N_{surface}$ and N_{inner} for commercially available rutile TiO_2 increase with a particle size decrease.[31] This means that smaller particles contain a larger number of surface defects but also contain a larger number of inner defects. This trade-off relation therefore results in lower $N_{surface}/N_{total}$ values and exhibits insufficient photocatalytic activity for commercially available TiO_2 (Figure 5e).

In contrast, as shown by the red symbol (Figure 9b), the data for HF(10)/P25 (sample **3**) does not follow the tendency for commercially available TiO_2. Its $N_{surface}$ is very large although the N_{inner} is very small. This means that these particles contain a relatively large number of surface defects despite a small number of inner defects, thus resulting in larger $N_{surface}/N_{total}$ value (Figure 5e). The smaller number of inner defects suppresses recombination of e^- and h^+, and the relatively large number of surface defects facilitates efficient nitro reduction, promoting highly efficient nitro reduction on the HF(10)/P25 catalyst. As shown by the blue symbol (Figure 9b), $N_{surface}$ of HF(15)/P25 (sample **4**) is lower than HF(10)/P25, because the treatment of P25 with higher concentration of HF decomposes surface structure and decreases the number of

dx.doi.org/10.1021/cs400532p | ACS Catal. 2013, 3, 2318–2326

surface defects. The result is consistent with the activity data (Figure 5e).

The above data suggest that the rutile particles isolated from P25 possess a defect distribution different from that of rutile TiO_2 synthesized by the wet process. The large $N_{surface}/N_{total}$ character specific for the isolated particles facilitates efficient nitro-to-amine reduction. The dry process (flame pyrolysis of gaseous $TiCl_4$) definitely creates such a specific defect distribution and produces rutile particles with high $N_{surface}/N_{total}$ value. It is, however, unclear yet how the specific defect distribution is created on the particles by the dry process. Nevertheless, the obtained findings clearly suggest that photocatalytic hydrogenation of nitroaromatics occurs very efficiently on the rutile particles with larger $N_{surface}/N_{total}$ value, and the dry process successfully creates rutile particles with a desirable defect distribution.

CONCLUSION

We found that rutile TiO_2 particles, isolated from P25 by HF treatment, promote highly efficient photocatalytic hydrogenation of nitroaromatics, with an activity higher than that of commercially available rutile TiO_2 synthesized by the wet process. The activity of rutile particles depends on the number of defects on the particles. The inner defect behaves as the deactivation site for the recombination of photoformed e^- and h^+ pairs, whereas the surface defect behaves as the active reduction site for nitroaromatics as well as the deactivation site. The catalyst with a larger number of surface defects relative to the number of total defects ($N_{surface}/N_{total}$) therefore exhibits higher activity. The P25 TiO_2 created by the dry process contains rutile particles with a high $N_{surface}/N_{total}$ ratio. This thus promotes efficient charge separation of the photoformed e^- and h^+ pairs and facilitates rapid nitro-to-amine reduction on the rutile particles isolated from P25 TiO_2. The recovery of rutile particles after HF treatment of P25 is only about 8%, which is one of the drawbacks for practical applications. Nevertheless, the results presented here may contribute to the design of more active photocatalyst for reduction reactions and may help open a new strategy toward green organic synthesis based on photocatalysis.

EXPERIMENTAL SECTION

Materials. All regents used were purchased from Wako, Tokyo Kasei, and Sigma-Aldrich, and used without further purification. Water was purified by the Milli Q system. P25 TiO_2 (JRC-TIO-4) was kindly supplied from the Catalyst Society of Japan. HF(x)/P25 was prepared as follows: P25 particles (1 g) were stirred in water (50 mL) with different concentrations of HF (x wt %) for 24 h at 298 K. The resulting powders were washed with water until the pH of the solution becomes about 7 and dried in vacuo for 12 h.

Photoreaction. Each respective substrate was dissolved in 2-PrOH solution. The solution and catalyst were added to a Pyrex glass tube (φ 12 mm; capacity, 20 mL), and the tube was sealed with a rubber septum cap. The catalyst was dispersed well by ultrasonication for 5 min, and N_2 was bubbled through the solution for 5 min. The tube was photoirradiated with magnetic stirring using a 2 kW Xe lamp (USHIO Inc.).[32] The wavelengths of the light irradiated to the solution are λ >300 nm because of the light absorption by the Pyrex glass tube. The intensity of light at 300−450 nm, which may mainly promote photoexcitation of TiO_2, was determined to be 27.3 W m^{-2}. The reaction was performed without the control of temperature; the temperature of solution during photoirradiation was about 303 K. After the reaction, the catalyst was recovered by centrifugation, and the resulting solution was analyzed by GC-FID. The substrate and product concentrations were calibrated with authentic samples. Analysis was performed at least three times, and the errors were ±0.2%. It is noted that the solubility of substrate and products in solution is sufficiently high, and the amount of them adsorbed onto the catalyst is negligible.

Analysis. XRD analysis was carried out on a Philips X'Pert-MPD spectrometer.[33] TEM observations were carried out using an FEI Tecnai G2 20ST analytical electron microscope operated at 200 kV.[34] DLS analysis was performed on a Horiba LB-500 dynamic light-scattering particle size analyzer.[35] The measurement was carried out with water containing respective TiO_2 particles (20 mg/L), after ultrasonication for 5 min. DRIFT spectra were measured on a FT/IR 610 system equipped with a DR-600B in situ cell (JASCO Corp.). DR UV−vis spectra were measured on an UV−vis spectrophotometer (JASCO Corp.; V-550 equipped with Integrated Sphere Apparatus ISV-469) with $BaSO_4$ as a reference.

ASSOCIATED CONTENT

Supporting Information

XRD patterns for TiO_2 (Figure S1), DR UV−vis spectra for TiO_2 (Figure S2), TEM images of HF(10)/P25 (Figure S3) and HF(15)/P25 (Figure S4), size distribution of TiO_2 particles (Figure S5), Time-dependent change in the aniline formation during photoreaction of nitrobenzene on respective TiO_2 (Figure S6). This material is available free of charge via the Internet at http://pubs.acs.org.

AUTHOR INFORMATION

Corresponding Author

*E-mail: shiraish@cheng.es.osaka-u.ac.jp.

Notes

The authors declare no competing financial interest.

ACKNOWLEDGMENTS

This work was supported by the Grant-in-Aid for Scientific Research (No. 23360349) from the Ministry of Education, Culture, Sports, Science and Technology, Japan (MEXT).

REFERENCES

(1) Downing, R. S.; Kunkeler, P. J.; van Bekkum, H. *Catal. Today* **1997**, *37*, 121−136.
(2) Burawoy, A.; Critchley, J. P. *Tetrahedron* **1959**, *5*, 340−351.
(3) Rylander, P. N. *Catalytic Hydrogenation in Organic Synthesis*; Academic Press,: New York, 1979; p 122.
(4) Corma, A.; Serna, P.; Concepción, P.; Calvino, J. J. *J. Am. Chem. Soc.* **2008**, *130*, 8748−8753.
(5) Reis, P. M.; Royo, B. *Tetrahedron Lett.* **2009**, *50*, 949−952.
(6) Corma, A.; Serna, P. *Science* **2006**, *313*, 332−334.
(7) Corma, A.; Concepción, P.; Serna, P. *Angew. Chem., Int. Ed.* **2007**, *46*, 7266−7269.
(8) Boronat, M.; Concepcion, P.; Corma, A.; González, S.; Illas, F.; Serna, P. *J. Am. Chem. Soc.* **2007**, *129*, 16230−16237.
(9) Mitsudome, T.; Mikami, Y.; Matoba, M.; Mizugaki, T.; Jitsukawa, K.; Kaneda, K. *Angew. Chem., Int. Ed.* **2012**, *51*, 136−139.
(10) Shiraishi, Y.; Togawa, Y.; Tsukamoto, D.; Tanaka, S.; Hirai, T. *ACS Catal.* **2012**, *2*, 2475−2481.
(11) Tanaka, K.; Capule, M. F. V.; Hisanaga, T. *Chem. Phys. Lett.* **1991**, *187*, 73−76.

(12) Ohtani, B.; Prieto-Mahaney, O. O.; Li, D.; Abe, R. *J. Photochem. Photobiol. A* **2010**, *216*, 179−182.
(13) Papageorgiou, A. C.; Beglitis, N. S.; Pang, C. L.; Teobaldi, G.; Cabailh, G.; Chen, Q.; Fisher, A. J.; Hofer, W. A.; Thornton, G. *Proc. Natl. Acad. Sci. U.S.A.* **2010**, *107*, 2391−2396.
(14) Rodriguez, J. A.; Jirsak, T.; Liu, G.; Hrbek, J.; Dvorak, J.; Maiti, A. *J. Am. Chem. Soc.* **2001**, *123*, 9597−9605.
(15) Dohnálek, Z.; Lyubinetsky, I.; Rousseau, R. *Prog. Surf. Sci.* **2010**, *85*, 161−205.
(16) Kirchnerova, J.; Herrera Cohen, M.-L.; Guy, C.; Klvana, D. *Appl. Catal., A* **2005**, *282*, 321−332.
(17) Sachtleben Chemie GmbH, Duisburg, Germany, June 24, 1994.
(18) Ohno, T.; Sarukawa, K.; Matsumura, M. *J. Phys. Chem. B* **2001**, *105*, 2417−2420.
(19) Ramis, G.; Busca, G.; Cristiani, C.; Lietti, L.; Forzatti, P.; Bregani, F. *Langmuir* **1992**, *8*, 1744−1749.
(20) Pillai, S. C.; Periyat, P.; George, R.; McCormack, D. E.; Seery, M. K.; Hayden, H.; Colreavy, J.; Corr, D.; Hinder, S. J. *J. Phys. Chem. C* **2007**, *111*, 1605−1611.
(21) Yu, J. C.; Yu, J.; Zhao, J. *Appl. Catal., B* **2002**, *36*, 31−43.
(22) Kitano, M.; Iyatani, K.; Tsujimaru, K.; Matsuoka, M.; Takeuchi, M.; Ueshima, M.; Thomas, J. M.; Anpo, M. *Top. Catal.* **2008**, *49*, 24−31.
(23) Ohno, T.; Sarukawa, K.; Tokieda, K.; Matsumura, M. *J. Catal.* **2001**, *203*, 82−86.
(24) Bickley, R. I.; Gonzalez-carreno, T.; Lees, J. S.; Palmisano, L.; Tilley, R. J. D. *J. Solid State Chem.* **1991**, *92*, 178−190.
(25) Kuang, Q.; Yang, S. *ACS Appl. Mater. Interfaces* **2013**, *5*, 3683−3690.
(26) Ahmad, I.; Dines, T. J.; Rochester, C. H.; Anderson, J. A. *J. Chem. Soc., Faraday Trans.* **1996**, *92*, 3225−3231.
(27) Kong, M.; Li, Y.; Chen, X.; Tian, T.; Fang, P.; Zheng, F.; Zhao, X. *J. Am. Chem. Soc.* **2011**, *133*, 16414−16417.
(28) Ikeda, S.; Sugiyama, N.; Murakami, S.; Kominami, H.; Kera, Y.; Noguchi, H.; Uosaki, K.; Torimoto, T.; Ohtani, B. *Phys. Chem. Chem. Phys.* **2003**, *5*, 778−783.
(29) Watanabe, T.; Honda, K. *J. Phys. Chem.* **1982**, *86*, 2617−2619.
(30) Murakami, N.; Prieto Mahaney, O. O.; Abe, R.; Torimoto, T.; Ohtani, B. *J. Phys. Chem. C* **2007**, *111*, 11927−11935.
(31) Yan, J.; Wu, G.; Guan, N.; Li, L.; Li, Z.; Cao, X. *Phys. Chem. Chem. Phys.* **2013**, *15*, 10978−10988.
(32) Shiraishi, Y.; Sugano, Y.; Tanaka, S.; Hirai, T. *Angew. Chem., Int. Ed.* **2010**, *49*, 1656−1660.
(33) Tsukamoto, D.; Shiraishi, Y.; Sugano, Y.; Ichikawa, S.; Tanaka, S.; Hirai, T. *J. Am. Chem. Soc.* **2012**, *134*, 6309−6315.
(34) Sugano, Y.; Shiraishi, Y.; Tsukamoto, D.; Ichikawa, S.; Tanaka, S.; Hirai, T. *Angew. Chem., Int. Ed.* **2013**, *52*, 5295−5299.
(35) Shiraishi, Y.; Tanaka, K.; Shirakawa, E.; Sugano, Y.; Ichikawa, S.; Tanaka, S.; Hirai, T. *Angew. Chem., Int. Ed.* **2013**, *52*, 8304−8308.